Atmos. Chem. Phys. Discuss., 14, 2675–2716, 2014
www.atmos-chem-phys-discuss.net/14/2675/2014/
doi:10.5194/acpd-14-2675-2014

Atmospheric Chemistry and Physics Discussions

Systematic satellite observations of the impact of aerosols from passive volcanic degassing on local cloud properties

S. K. Ebmeier[1], A. M. Sayer[2], R. G. Grainger[3], T. A. Mather[4], and E. Carboni[3]

[1]COMET/NCEO, School of Earth Sciences, University of Bristol, Park Street, Bristol, UK
[2]Goddard Earth Science Technology And Research (GESTAR), NASA Goddard Space Flight Center, Greenbelt, MD, USA
[3]COMET/NCEO, Atmospheric, Oceanic and Planetary Physics, University of Oxford, Parks Road, Oxford, UK
[4]COMET/NCEO, Department of Earth Sciences, University of Oxford, South Parks Road, Oxford, UK

Received: 22 November 2013 – Accepted: 16 January 2014 – Published: 27 January 2014

Correspondence to: S. K. Ebmeier (sk.ebmeier@bristol.ac.uk)

Published by Copernicus Publications on behalf of the European Geosciences Union.

Abstract

The impact of volcanic emissions is a significant source of uncertainty in estimations of aerosol indirect radiative forcing, especially with respect to emissions from passive degassing and minor explosions. Understanding the impact of volcanic emissions on indirect radiative forcing is important for assessing present day atmospheric properties and also to define the pre-industrial baseline to assess anthropogenic perturbations. We present observations of the time-averaged indirect aerosol effect within 200 km downwind of isolated island volcanoes in regions of low present-day aerosol burden using MODIS and AATSR data. Retrievals of aerosol and cloud properties at Kīlauea (Hawai'i), Yasur (Vanuatu) and Piton de la Fournaise (Réunion) are rotated about the volcanic vent according to wind direction, so that retrievals downwind of the volcano can be averaged to improve signal to noise ratio. The emissions from all three volcanoes, including those from passive degassing, strombolian activity and minor explosions lead to measurably increased aerosol optical depth downwind of the active vent. Average cloud droplet effective radius is lower downwind of the volcano in all cases, with the peak difference in effective radius of 4–8 µm at the different volcanoes. A comparison of these observations with cloud properties at isolated islands with no significant source of aerosol suggests that these patterns are not purely orographic in origin. This approach sets out a first step for the systematic measurement of the effects of present day low altitude volcanic emissions on cloud properties. Our observations of unpolluted, isolated marine settings may also capture processes similar to those in the pre-industrial marine atmosphere.

ACPD
14, 2675–2716, 2014

1 Background

1.1 Aerosol indirect effects

Aerosols affect the Earth's albedo directly, through the absorption and scattering of solar radiation, and indirectly, by altering the properties of clouds. Elevated levels of aerosol potentially lead to higher number densities of cloud condensation nucleii (CCN), and for an air parcel with a fixed mass of water, result in higher droplet concentrations and consequently lower droplet radius and higher albedo (Twomey or first indirect effect; Twomey, 1977). In addition, smaller cloud droplets result in the suppression of precipitation and therefore longer cloud lifetime, i.e. higher albedo (second indirect effect, Albrecht, 1989). The presence of aerosol in a cloud may also cause the evaporation of cloud droplets due to aerosol absorption of solar radiation and several less well-understood perturbations to droplet character in mixed phase clouds (e.g. Hansen et al., 1997). Aerosol indirect effects are reviewed by Lohmann et al. (2005).

The contributions of indirect effects to the Earth's radiative balance are strong, yet also highly uncertain. Carslaw et al. (2013) suggest that 45 % of variance in post-1750 aerosol forcing is from natural sources, which are hard to isolate and measure in the polluted present-day atmosphere (Andreae et al., 2007). The response of cloud properties to additional CCN is non-linear: excess CCN has the greatest effect on albedo when background levels of aerosol are lowest (e.g. Lohmann et al., 2005). Present day aerosol indirect effects are therefore expected to most closely match pre-industrial processes in remote marine environments where pollution levels are low (Andreae et al., 2007).

Direct observations of aerosol indirect effects have so far been dominated by measurements of ship tracks (e.g. Durkee et al., 2000; Ackerman et al., 2000; Campmany et al., 2009; Christensen and Stephens, 2011; Peters et al., 2011). Aerosol from shipping provides an ideal experiment for isolating the impact of aerosols, as the polluted clouds are otherwise identical in origin and thickness to clean clouds in the surrounding cloud deck. For the case of ship tracks, the occurrence and albedo resulting from

ACPD
14, 2675–2716, 2014

additional aerosol has been shown to depend on pre-existing cloud structure, height and humidity (e.g. Chen et al., 2012). The impact of excess aerosol from sources on the continents or coasts are harder to isolate because continental cloud formations vary over shorter distances, and are also systematically thinner and drier than oceanic clouds (e.g. Brenguier et al., 2003).

1.2 Volcanic indirect effect

The impact of volcanogenic aerosol on cloud properties depends on injection height into the atmosphere, pre-existing aerosol burden and synoptic conditions. Explosive eruptions can inject aerosol directly into the stratosphere (as coarse particles from fragmented magma, vent wall erosion and condensation of magmatic gases) and provide the gas-phase reactants for the production of finer aerosols in the plume or ambient atmosphere (e.g. sulphate aerosol). Direct and indirect aerosol effects associated with explosive eruption products in the stratosphere have been relatively well characterised (Sassen, 1992; Robock, 2002; Schmidt et al., 2010). However, the role of aerosol in the troposphere from "passive" degassing and minor eruptions is less well understood (Mather et al., 2003; Oppenheimer et al., 2011). Time-averaged emissions from passive degassing make up a high proportion of the volcanic SO_2 flux to the atmosphere (Andres and Kasgnoc, 1998; Halmer et al., 2002; Mather et al., 2003). Volcanogenic aerosols in the troposphere are expected to be dominated by sulphate aerosol (SO_4^{2-}) produced from the oxidation of SO_2 by OH^-, H_2O_2 or O_3 above the boundary layer, or in high temperature reactions of SO_2 or H_2S in the volcanic vent (e.g. Mather et al., 2006). Ambient temperature SO_2 reactions can take place over several days, so the impact of volcanic aerosol on number density of CCN may extend hundreds of kilometres away from the aerosol source (Eatough et al., 1995).

Although the flux of volcanic aerosol to the present day troposphere is lower than the anthropogenic flux, its impact on radiative budget may be disproportionately significant, as volcanic gases are commonly emitted at heights above the boundary layer into the free troposphere, so resulting aerosol lifetimes may be longer (e.g. Graf et al.,

ACPD
14, 2675–2716, 2014

1998). Though not as significant as the uncertainties in aerosol fluxes from biomass burning and anthropogenic SO_4^{2-} sources, volcanic aerosol remains a source of uncertainty in global model simulations of present day CCN (e.g. Lee et al., 2013). As volcanic emissions contribute a lower proportion of CCN to the atmosphere today than in pre-industrial times, the quantification of the volcanogenic indirect effect is particularly important for estimating the baseline cloud radiative state (Schmidt et al., 2012). Of the natural emmisions thought to contribute 45 % of variance to estimations of global mean forcing uncertainty, volcanic SO_2 emissions have the greatest potential range (Carslaw et al., 2013).

Ground-based measurements of plumes near passively degassing vents have captured (1) an abundance of SO_4^{2-} aerosol larger than the critical diameter to act as a CCN at typical supersaturations (e.g. Allen et al., 2002; Martin et al., 2008; Mather et al., 2012) and (2) particle growth attributed to the condensation of water vapour onto sulphate particles between 0 and 20 km distance from the vent (Villarica, Chile; Mather et al., 2004). Satellite remote sensing studies have gone a step further to measuring a volcanic indirect effect during periods of high flux degassing. Gassó (2008) shows alteration to stratocumulus properties ("volcano tracks") in Moderate Resolution Imaging Spectroradiometer (MODIS) and Advanced Microwave Scanning Radiometer – Earth Observing System (AMSR-E) images where large plumes from volcanoes in the South Sandwich islands and the Aleutians interact with marine boundary layer clouds. Instances of increased cloud brightness in the presence of an obvious volcanic plume were identified by browsing MODIS visible images from six months in 2006, and cloud property data from a few selected days were analysed to demonstrate first and second indirect effects in the volcano tracks. Yuan et al. (2011) have also assessed the impact of high degassing flux associated with a new vent opening at Halema'uma'u crater, Hawai'i, in 2008 on trade cumulus clouds. The authors compare retrievals of cloud and aerosol properties averaged over three months from inside the Halema'uma'u plume to properties both outside the plume over the same time, and to the average properties

ACPD
14, 2675–2716, 2014

retrieved over a much longer period. Both studies (Gassó, 2008; Yuan et al., 2011) find evidence for increased albedo and for increased cloud lifetime in marine clouds.

1.3 Motivation and aim

Although volcanic aerosol acting as CCN has been observed at several volcanoes (e.g., Mather et al., 2004; Gassó, 2008; Yuan et al., 2011, etc.), it has not yet been measured either on a global scale or over extended periods of time. More representative measurements are important for testing and verifying the predictions of global microphysical aerosol models (e.g. Martin et al., 2006; Dentener et al., 2006; Schmidt et al., 2012), that rely on inventories of sulphur emission such as Andres and Kasgnoc (1998).

As measurements of the volcanic indirect effect so far have been made over short periods of time (3–5 months) and during elevated activity (e.g. frequent MODIS thermal anomalies at Montagu and Saunders Islands, Gassó (2008); Halema'uma'u vent opening see Sect. 3.3, Yuan et al., 2011), they are not likely to be representative of the long-term impact of "background" activity on tropospheric cloud properties. The automated detection of a volcanic indirect effect, such as that developed by Campmany et al. (2009) for the detection of ship tracks, would allow us to build up a more complete picture of the global significance of volcanic degassing. However, it is harder to identify a natural experiment where clean and volcanically polluted clouds of otherwise identical properties can be compared. Unlike pollutants from shipping, which all have similar composition and are emitted at low elevation, aerosol sources may vary between different volcanoes. Volcanic aerosols are released (or injected) into the atmosphere at different heights, from just above sea-level up to several kilometres, and source strength and exact type of aerosol varies with the character of volcanic activity. Most volcanoes are associated with mountain ranges that exert control on local climate and cloud formation, so that cloud properties upwind and downwind of the volcano are systematically different. Aerosols generated over land are also more diverse in origin,

ACPD
14, 2675–2716, 2014

chemistry and concentration than those formed over the oceans. The identification of a volcanic indirect effect is therefore less suited to a single algorithm than ship tracks.

We present an approach for detecting a volcanic indirect effect for the particular case of isolated, active volcanic islands. These marine environments have among the lowest aerosol burden in the world (Fig. 1) and are likely to represent the most reasonable present-day analogue for pre-industrial conditions. We use averages of 6–10 yr of data and make no selection on the basis of activity, so that our results may be considered representative of the net effect of volcanic emissions on clouds at a particular volcano. We aim to capture the volcanic indirect effect associated with "background activity", that is, periods when degassing or other persistent activity results in aerosol emission deep in the atmosphere and that may not result in visibly identifiable "volcano tracks".

2 Satellite data

We use aerosol and cloud properties retrieved from data from MODIS on satellites Aqua and Terra and from ESA's Advanced Along-Track Scanning Radiometer (AATSR) on ENVISAT between 2002 and 2008. We use aerosol optical depth at 550 nm, (AOD, Remer et al., 2005) and various cloud properties (e.g., cloud optical depth, COD, cloud droplet effective radius, CER, Platnick et al., 2003; Ackerman et al., 2008) from MODIS Collection 5 Atmosphere Level 2 Joint Product (MODATML2 and MYDATML2). We select MODIS cloud retrievals where cloud fraction from MODIS cloud product is > 0.2, and Quality Assurance (QA) values are > 0. For aerosol retrievals, we also require QA > 0, as well as the aerosol product cloud fraction to be < 0.8. We also use the Oxford-RAL Retrieval of Aerosol and Clouds (ORAC GRAPE dataset) from AATSR data (Thomas et al., 2009; Sayer et al., 2010; Poulsen et al., 2011), including retrievals of aerosol and cloud optical depth and cloud droplet effective radius. Cloud fraction, cloud top pressure and temperature were used to distinguish between retrievals from different atmospheric heights and under different synoptic conditions. We restrict our observations to liquid water rather than ice clouds and to data where cloud top pres-

ACPD
14, 2675–2716, 2014

sures were < 440 mb. All properties are resampled to a grid of 10 km resolution to simplify comparison, with sampling rate of around 100–300 per bin.

We select data within a square of side length 4° (up to 600 km, depending on latitude) centred on the volcanic vent. We then convert the latitude-longitude for each retrieval pixel into polar coordinates with the origin located on the volcano's summit, as recorded in the Smithsonian database (Siebert and Simkin, 2002). We use horizontal wind velocity components from the European Centre for Medium-Range Weather Forecasts (ECMWF) (e.g. Dee et al., 2011) to rotate the aerosol and cloud properties according to wind direction, so that they can be plotted according to their expected position upwind or downwind relative to the volcano. Horizontal wind velocity components are chosen for the time of day closest to the satellite overflight time. We assume that gases and aerosols are emitted from each volcano at approximately its summit height, so wind data are selected for a pressure level expected to lie just above this height. We use the volcano's summit or the most active vent as the origin for rotation because for all cases here, gases were emitted from multiple vents contributing varying proportions of total aerosol emissions.

The resulting averaged images of rotated cloud and aerosol properties allow us to examine systematic trends that are not apparent in the properties retrieved for individual days, or in the stack of all our data before rotation. Unlike previous studies at periods of high SO_2 emission (e.g. Gassó, 2008; Yuan et al., 2011), volcano tracks were rarely identifiable in individual MODIS visible images or in cloud properties on specific dates. The temporal variability of aerosol optical depth (AOD) is also such that days when volcanic activity was elevated according to ground reports cannot be identified from time series of mean daily AOD (see Sect. 3.3). For the satellite data used in this study, retrieval of cloud and aerosol properties are mutually exclusive, as aerosols are retrieved only in clear sky conditions. It is therefore not possible to investigate the relationship between the amount of aerosol and cloud properties directly. We consider the average aerosol and cloud properties across several years to draw general con-

ACPD
14, 2675–2716, 2014

clusions about their relationship, in particular with respect to their position upwind or downwind of an active volcanic vent.

We select target volcanoes for our study where sources of uncertainty are expected to be low, to allow us to identify low magnitude perturbations in cloud properties. Uncertainties in AOD retrieved from MODIS data over land are thought to be on average three times greater than over water, where models of surface reflectance are better (Remer et al., 2005). We therefore focus our study on isolated volcanic islands, avoiding the higher retrieval uncertainties, greater variability in cloud characteristics associated with continents and the systematic dependence of cloud form on wind over coastlines or high topography. The ideal target for our approach is a small and low island volcano, with a high, persistent degassing flux and located a long way from other sources of tropospheric aerosol, such as cities, heavy industry or shipping.

We choose three isolated, persistently if variably active volcanoes to test our approach (Fig. 1): Kīlauea (Hawai'i), Yasur (Vanuatu) and Piton de la Fournaise (Réunion). As described above, measurements of a volcanic indirect effect downwind of Kīlauea during the opening of the new Halema'uma'u vent have previously been made by Yuan et al. (2011). This study differs in that although all three systems are mafic and persistently active, there are significant differences in degassing flux and the character of eruptive activity between them (Table 1).

A volcanic indirect effect is expected to be characterised by (a) elevated AOD and (b) depressed CER downwind of the volcanic source relative to upwind. However, we also expect an orographic effect over isolated peaks in topography (e.g. Jiusto, 1967) to cause a systematic upwind/downwind difference in cloud droplet radius: when moist air is lifted up over an island it expands, cools and condenses, potentially causing precipitation on the windward side of the island. We therefore also consider data for three "control" islands known not to emit volcanogic aerosol or precursor gases (Tristan da Cunha in the South Atlantic; Ofu-olosega, American Samoa and Fiji, both in the South Pacific – Table 1), chosen for their similarities in topographic height and diameter to our

ACPD
14, 2675–2716, 2014

target volcanoes (Fig. 2), and their isolation from sources of volcanic or anthropogenic aerosol.

3 Results

We observe differences between downwind and upwind aerosol and cloud properties at the volcanoes far greater than at the control sites. AOD is elevated and cloud droplet effective radius suppressed at all three volcanoes, and at Kīlauea and possibly Yasur we also observe a slight relative increase in cloud optical thickness downwind. Although in some cases uncertainties are expected to be introduced by regional trends in cloud properties and the use of coarse resolution ECMWF wind fields, we are confident that upwind-downwind difference in cloud properties are dominated by a volcanic indirect effect (Fig. 2). In contrast, we see no elevation in AOD and no depression in CER at the control sites, except for a limited ($< 1\,\mu m$) effect within 100 km downwind of Tristan da Cunha (Sect. 3.2). Degassing processes and patterns are notably different at each of the volcanoes, and we discuss results from each volcano below with reference to other measurements of volcanic aerosol and prevailing meteorological conditions (Sects. 3.3–3.5).

3.1 General features of rotated cloud and aerosol properties

Aerosol and cloud optical depth retrievals are consistent between MODIS Terra and Aqua as well as AATSR: all instruments show elevated AOD downwind of the volcanoes, but not control islands, and elevated cloud optical depth over all islands (Aqua data are shown in Fig. 2, and a comparison of all three instruments at Réunion is shown in Fig. 3a and c). Rotated and averaged AATSR retrievals have higher standard errors than for MODIS due to smaller sample size. All instruments show similar patterns in CER, lower droplet size downwind of the volcano, although the absolute values for effective radii are greater for MODIS than AATSR retrievals (upwind average of 17 µm

ACPD
14, 2675–2716, 2014

and 14 µm, respectively at Piton de la Fournaise, Fig. 3b). This is due to the difference between the wavelengths used by the MODIS and AATSR retrieval algorithms. The shorter wavelength used by AATSR penetrates deeper into the clouds, so will sample smaller cloud droplets in a non-precipitating cloud, which typically have increasing cloud droplet size with height (Platnick, 2000; Sayer et al., 2011).

The profiles shown in Fig. 2b, f and j show peak AOD downwind of the volcano, immediately beyond the edge of the island in each case. The larger error bars over the land for both cloud and aerosol properties are the result of (a) fewer data points contributing to the mean (i.e. an arc of $\frac{\pi}{2}$ is smaller closer to the volcano) and (b) a greater spread in the retrieval values made over land. Observations made beyond the extent of the island, indicated by dashed lines showing average island diameter on Fig. 2, are most robust.

The higher uncertainty in retrievals made over land may also contribute to the "anticipation" of the volcano, seen, for example, ∼ 50 km upwind of Kīlauea in Fig. 2b and Yasur in Fig. 2f. When the aerosol data are rotated, any error in the ECMWF wind direction smears out the upwind-downwind difference radially around the volcano. Errors introduced by this effect are greatest where local wind fields are least well represented by the ECMWF wind fields (spatial resolution = 1.5°). As we use the wind velocities as close as possible to the volcano itself, uncertainties will generally increase with distance from it. However, isolated topographic peaks, such as these volcanoes, introduce perturbations to the regional wind fields, resulting in local turbulence near the volcano itself. These uncertainties could be avoided by carrying out trajectory analysis of air parcels from the volcano's summit rather than assuming that wind fields are uniform. This would also allow us to track the impact of volcanic aerosol at greater distances from the volcano, but would require the integration of higher resolution wind fields and add complexity to the automation.

For most of the volcanoes and islands shown in Fig. 2, cloud and aerosol properties upwind and downwind at distances > 200 km are similar, but at Yasur there are linear trends in properties from upwind to downwind. We attribute this to differences in

ACPD
14, 2675–2716, 2014

average cloud properties on the scale of hundreds of kilometres, introducing a ramp to the rotated data due to very consistent wind direction. This is further illustrated by the upwind-downwind difference in numbers of cloud retrievals (number of retrievals flagged as "cloud" and where cloud fraction > 0.2 are shown in Fig. 4). At Yasur, where prevailing winds blow to the northwest, there were many more cloud retrievals downwind than upwind, though cloud optical depth remained similar. There were also minor regional trends aligned with the prevailing wind direction in the areas surrounding American Samoa and Tristan da Cuhna.

3.2 Distinguishing between orographic and volcanic effects

Orographic clouds form when moist air is forced upwards by high topography so that it expands and cools below its saturation point. Their form depends on relative humidity, wind speed and the height and geometry of topography. At high humidity and lower wind speeds, droplets condense above the windward slopes of a mountain, sometimes causing orographic precipitation. Wave clouds may also form in perpendicular bands downwind of high topography. At isolated, steep sided mountains high wind speeds can cause local uplifting on the upper slopes in the lee side of the mountain ("banner cloud"). As the formation of orographic cloud is controlled by wind strength and direction, its presence is expected to introduce systematic features to our rotated cloud properties.

For a tall, isolated island, orographic clouds may form (1) over high land upwind of the summit and (2) at the crests of lee waves (rotor and lenticular clouds), downwind and extending hundreds of kilometres away from the island (e.g. Houze, 1994). We observe elevated cloud optical depth in our stacked cloud property data over the islands with high topography (Kīlauea, Réunion, Fiji and to some extent Tristan da Cunha). Cloud optical depth is elevated immediately upwind of the island's summit and remains high over land downwind. Any difference in optical depth between the windward and lee sides of the islands at greater distance is very low, suggesting that the contribution of wave clouds to the average values is small.

ACPD
14, 2675–2716, 2014

Orographic cloud has smaller droplets at a higher density than marine clouds. For example, Jiusto's (1967) aircraft sampling of both marine and orographic cloud upwind of Kīlauea, found that marine clouds had an average radius of $22 \pm 3\,\mu m$, (droplet concentration $45 \pm 22\,cm^{-3}$) while clouds on the flanks of Mauna Loa had an average radius of $14 \pm 3\,\mu m$ (droplet concentration $100 \pm 50\,cm^{-3}$). Although the values are not directly comparable, we find a similar decrease in droplet size (22 to 18 µm) on the windward side of Big Island Hawai'i. However, cloud droplet effective radius does not reach its minimum value (14 µm) until almost 100 km downwind, and remains lower than upwind values until almost 400 km from land (see Fig. 2). We see no such effect in clouds downwind from Fiji (also ∼ 100 km across and in the path of easterly trade winds, but lower in elevation) or American Samoa, but Tristan da Cunha shows a small decrease in droplet size. We note that this decrease in CER downwind of Tristan da Cunha correlates well with a downwind increase in cloud optical depth. At the active volcanoes (e.g. Fig. 2c or k), downwind droplet radius remains low at greater distances from the vent than cloud optical depth remains elevated. Cloud droplet radius, though influenced by orographic processes, is more strongly affected by volcanogenic aerosol at Kīlauea, Yasur and Piton de la Fournaise.

3.3 Kīlauea, Hawai'i

Kīlauea is the most active of the Hawaiian volcanoes and contributes 4 % of the total emissions in Andres and Kasgnoc's (1998) time-averaged compilation of emissions from 49 continuously erupting volcanoes. Activity is effusive, and generally split between the East Rift zone, where lava effusion has been semi-continuous since 1983, and periodic degassing, lava pond activity and occasional small explosions at the volcano's summit. The emission of SO_2 is measured with miniature spectrometers independently at the East Rift Zone and summit by the United States Geological Survey (USGS) using regular vehicle-based traverses and intermittent stationary scanning measurements (Elias and Sutton, 2012). Prior to 2008 approximately 90 % of SO_2 emissions were from the East Rift Zone, and between the 1970's and 1990's the East

ACPD
14, 2675–2716, 2014

Rift Zone is thought to have been the second largest sporadic volcanic source of SO_2 (Andres and Kasgnoc, 1998). During our period of observation, between 2002 and the beginning of 2008, average total annual emissions were 6.58×10^5 Mg yr^{-1} (Elias and Sutton, 2012). A comparison of the USGS ground-based measurements with MODIS AOD prior to 2008 for days where both measurements were possible (61 days) does not show a relationship between them (Fig. 5), perhaps due to the time difference between the measurements, the lag between SO_2 emission and aerosol formation or processes that affect the concentrations of aerosols such as dilution.

The opening of a new vent at Halemau'ma'u crater in 2008 was accompanied by a rise in total SO_2 flux to 7000 t day^{-1}, constituting a doubling of annual SO_2 emission rate from 2007 to 2008. Since 2008 summit emissions have steadily increased as a proportion of total SO_2 emission from Kīlauea, though total SO_2 emission had dropped to $\sim$ 2000 t day^{-1} by 2010 (Elias and Sutton, 2012). Yuan et al. (2011)'s measurements of the Halema'uma'u 2008 plume demonstrate a significant increase in cloud fraction and perturbation to cloud properties (a) inside the aerosol plume, relative to outside and (b) in 2008 during elevated emission, relative to the mean values for the 11 yr Terra archive. On 17 July 2008 Yuan et al. (2011) find an average background value of CER of 18 µm, reduced to $\sim$ 13 µm within the aerosol plume 800–1000 km downwind of Kīlauea. We find a similar magnitude of reduction in CER over a much smaller area (just $\sim$ 70 km downwind) in averaged data from 2002–2007, when degassing fluxes were lower (Fig. 2).

Sulphates dominate the compositions of aerosols measured at Kīlauea's summit (modal diameter 0.44 µm), and make up $\sim$ 1 % by mass of plume SO_2 concentrations (Mather et al., 2012). Porter et al. (2002) made sun photometer and LiDAR measurements of SO_4^{2-} 9 km downwind of a vent on the East Rift Zone in 2001, and found an aerosol dry mass flux rate of 53 t day^{-1} and infered a half life of 6 h for SO_2 in the plume. Assuming an average wind speed of range 5–10 m s^{-1}, if correct and broadly applicable in different atmospheric conditions, this implies that SO_2 mass falls below 10 % of its original value by a distance of 90–180 km downwind. Our estimations of av-

ACPD
14, 2675–2716, 2014

erage AOD place peak values at ~ 100 km downwind of Kīlauea's summit, consistent with oxidation of SO_2 as the primary source of aerosol.

Aerosol plume dispersal in Hawai'i is dominated by relatively stable trade winds from the north-east, and clouds are mostly trade cumuli, which are typically capped by the trade wind inversion at a height of a few kilometres. Although Kīlauea's summit elevation is only 1222 m, it overlaps the lower flanks of the much larger, but less active, Mauna Loa (4170 m). The impact of orographic cloud formation and precipitation is therefore likely to be more significant at Hawaii that any of the other examples considered here. There is a notable difference in the number of MODIS retrievals flagged as cloud downwind relative to upwind (retrievals with cloud fraction > 0.2 are shown in Fig. 4). More cloud retrievals were made downwind of Kīlauea, with the difference peaking at a distance of about 60 km downwind of the vent. Both cloud seeding associated with volcanic aerosol and the formation of orographic clouds are likely to contribute to this effect.

3.4 Yasur, Vanuatu

Yasur is the southernmost of the Vanuatu island arc's active volcanoes and exhibits almost continuous Strombolian to Vulcanian activity in an eruption that has lasted at least 300 yr. Magmatic gases, mostly SO_2, are continuously released from three vents in Yasur's crater and typically rise to heights of 700–900 m before being carried to the northwest by trade winds (Bani et al., 2012). Measurements made by Bani and Lardy (2007) and Bani et al. (2012) on 33 different days between 2004 and 2008 find an average degassing flux of 633 Mg day^{-1} SO_2 (standard deviation of daily measurements = 270 Mg day^{-1}). Bani and Lardy (2007) estimate that in 2004–5 Yasur contributed 1–2 % of estimated global time-averaged volcanic SO_2 emissions to the troposphere, close to Andres and Kasgnoc (1998)'s estimation of 3 % pre-1990s.

The nearest other aerosol sources to Yasur are just under 400 km away, at the volcanoes of Lopevi (156 t day^{-1} SO_2) and Ambrym (5440 t day^{-1} SO_2) (Bani et al., 2012). Yasur is close to being a sea-level point SO_2 source, with a summit elevation of just

ACPD
14, 2675–2716, 2014

361 m. We therefore expect any orographic effects to be minimal. There are also no indications of orographic clouds in rotated cloud properties at the small, remote islands in American Samoa (Ofu-olosega, elevation 639 m) used as "control" sites.

We measure elevated AOD (e.g. 0.13 for MODIS Aqua) downwind of Yasur, relative to that upwind (0.09), a difference that persists 400 km away from the vent. Ground based SO_2 measurements at Yasur have been too infrequent (Bani et al., 2012) to allow a useful comparison with AOD retrieved from MODIS data. There is also a net difference in cloud droplet radius between the downwind and upwind sectors (−3 µm, MODIS Aqua). Although most of this difference can be attributed to the impact of excess aerosol from Yasur, this is superimposed on a regional trend in aerosol.

3.5 Piton de la Fournaise, Réunion

Piton de la Fournaise, Réunion, differs from the previous two examples in that intra-eruptive SO_2 flux is low (Khokhar et al., 2005; Di Muro et al., 2012). However, on average Piton de la Fournaise erupts or experiences an intrusion once every 8 months (Peltier et al., 2009). Eruptions are sometimes associated with measurable SO_2 emission (Khokhar et al., 2005; Bhugwant et al., 2009), and emission is of longer duration during periods of distal lava effusion when lava entering the sea also results in a high flux of water vapour to the atmosphere (e.g. Gouhier and Coppola, 2011). Between eruptions, degassing is primarily from low temperature fumeroles and fractures around the active summit crater (Di Muro et al., 2012). Again unlike Kīlauea and Yasur, these weak emissions are dominated by water vapour, and hydrogen sulphide (H_2S) is the main sulphur species (Di Muro et al., 2012).

Piton de la Fournaise is the only one of the volcanoes investigated here that is likely to have had a high SO_2 flux associated with explosive eruption. The SO_2 released during the collapse of the Dolomieu crater in April 2007 (estimated to be 935 ± 244 kilotons by Gouhier and Coppola, 2011) rose quickly to heights > 3000 m (above the trade winds), and reached distances of 800–1000 km away from Réunion within days (Tulet and Villeneuve, 2011). Where SO_2 emission accompanies explosions, and aerosol is

ACPD
14, 2675–2716, 2014

carried above the trade winds there will presumably be excess aerosol from plume material settling out spread over a wider area, further from the volcano than for lower altitude plumes. By distances of ∼ 1000 km, the plume from this event reached heights of around 10 000 m a.s.l. (Tulet and Villeneuve, 2011). Piton de la Fournaise's other six eruptions between 2002 and 2008 (Siebert et al., 2010) were all less explosive, emitting aerosol lower into the atmosphere.

Our observations capture the impact of aerosol deep in the atmosphere, particularly on boundary layer clouds, and will therefore be dominantly affected by low altitude aerosol emission. However, our observations of the volcanic indirect effect are not limited to inter-eruptive emission. In Fig. 7 aerosol and cloud properties are split according to whether or not Piton de la Fournaise was erupting (as recorded in the Smithsonian database Siebert and Simkin, 2002). Aerosol is elevated all around the volcano during periods of eruption (compare Fig. 7a and b), but particularly in the downwind quadrant. Similarly, cloud droplet radius is lowest during periods of eruption in the downwind sector (compare Fig. 7c and d). Time-averaged data from 2002–2007 show a net effect of elevated AOD downwind of the volcano (0.12 relative to upwind 0.10 at ∼ 50 km distance from the volcano's summit). The CER of clouds within ∼ 100 km downwind of the volcano has a minimum value of 14 µm, relative to an upwind average of 21 µm (Fig. 2).

4 Discussion

4.1 Observations of volcanic aerosol

In remote parts of the oceans, primary sea spray aerosol dominates aerosol populations (e.g. Sayer et al., 2012; Smirnov et al., 2011; Huang et al., 2010). The linear relationships between mean daily AOD and surface wind speeds within 50 km radius of the volcanoes shown in Fig. 6 are as expected where sea spray aerosol is the most important background aerosol. The slopes of the linear regression between AOD and wind speed take values ranging from 0.003–0.005 for Kīlauea, Yasur and Réunion, re-

ACPD
14, 2675–2716, 2014

spectively in Fig. 6, Table 3. This is within the range found by Smirnov et al. (2011) from examination of ship-borne sun photometer aerosol optical depth measurements and near surface wind speeds (0.004–0.005). The strength of the AOD-wind relationships found from the MODIS retrievals may be underestimations, as the Collection 5 MODIS algorithm has a positive bias at low wind speeds and negative bias at high wind speeds (Sayer et al., 2010; Shi et al., 2011).

We attribute the differences in AOD upwind and downwind of the volcano to the contribution of volcanic aerosol alone, as the production of sea spray aerosol is likely to be similar upwind and downwind. Aerosol from the islands (e.g. organic carbon or mineral dust) would also produce a peak in optical depth over the island itself rather than 10's–100's km downwind as shown in Fig. 2. Maximum AOD occurs at about 100 km, 40 km and 50 km downwind of the expected source at Kīlauea, Yasur and Piton de la Fournaise, respectively. At Kīlauea and Yasur AOD remains elevated as far as 400 km downwind of the volcano's summit, while at Piton de la Fournaise, AOD has returned to upwind levels by a distance of ∼ 100 km. Although all three volcanoes are mafic and persistently active, their modes of gas and aerosol emission differ. At Kīlauea, SO_2 emission is passive and accompanies long-lived lava flows and lava lake activity, while at Yasur it varies in flux and composition according the stage of Strombolian explosion. Piton de la Fournaise has a very low inter-eruptive flux, but SO_2 emission accompanies frequent minor explosions and lava flows.

Time series of daily AOD from MODIS data all show a large day to day variability, which depends to some extent on wind speed (e.g. Fig. 6). This is in keeping with our expectations that daily AOD (both background and volcanogenic) is heavily dependent on synoptic and local meteorological conditions (see Sect. 4.3). A comparison of net downwind aerosol at the three volcanoes shows a general correlation between downwind AOD and average "background" or inter-eruptive SO_2 flux (e.g. Tables 1 and 2).

ACPD
14, 2675–2716, 2014

4.2 Evidence for a volcanic indirect effect

We use cloud optical depth and droplet effective radius to distinguish between the alteration of cloud properties due to volcanic aerosol and systematic differences in cloud properties caused by other phenomena.

Cloud optical depth is generally higher over the active volcanoes than the inactive islands, and is also slightly higher downwind than upwind. This could indicate an increase in cloud lifetime due to drizzle suppression (e.g. Lohmann et al., 2005), but it may also be the consequence of orographic cloud formation downwind or the contribution of cooling and condensing water vapour emitted from the volcano. Water vapour flux at Yasur is higher than $13 \times 10^3\,\mathrm{t\,day^{-1}}$ (Métrich et al., 2011). Emissions of water vapour into the atmosphere at Kīlauea and Piton de la Fournaise will be even higher due to the additional contribution of evaporated seawater where lava flows meet the sea (e.g. Edmonds and Gerlach, 2006; Gouhier and Coppola, 2011). Liquid water path derived from retrievals of cloud optical depth and CER reaches its peak value within ~ 50 km of the volcanic vents and is very slightly elevated downwind relative to upwind. Although they may be taking place, secondary indirect effects are not likely to be the only or most important contributing factor to elevated downwind cloud optical depth.

The anticorrelation between AOD and CER values downwind of the degassing volcanoes provides strong evidence for a volcanic first indirect effect. At all the active volcanoes minimum CER is found at similar downwind distance in averaged retrieval data as peak AOD. The difference between background (upwind) CER and the minimum value found downwind is greatest at Kīlauea (−7 µm, decrease of 32 %) and lower at Yasur and Piton de la Fournaise (both −4 µm, decrease of 18 %) in Terra retreivals. This difference far exceeds the expected uncertainty in MODIS Terra CER retreivals of 2–3.5 % (Platnick et al., 2003).

In common with the persistent downwind elevation in AOD described above, CER at Kīlauea and Yasur remains lower than upwind values at least as far as 400 km down-

ACPD
14, 2675–2716, 2014

wind, while CER returns to its average upwind value within 100 km at Réunion. Droplets in "clean" clouds upwind of the volcanoes have average effective radii of 21–22 µm.

In spite of the strong correlation, our measurements do not allow a direct measurement of the Twomey effect because retrievals of aerosol and cloud properties from MODIS and AATSR data are mutually exclusive (i.e. aerosol properties are retrieved only where pixels are not flagged as cloud). This may mean that there are differences between the meteorological conditions sampled by cloud and aerosol retrievals. Volcanic emissions themselves are independent of synoptic conditions, but oxidising agents and reaction rates for the formation of SO_4^{2-} from SO_2 are dependent on atmospheric conditions such as supersaturation and light levels (Eatough et al., 1995). The formation of aerosol may take place in a different manner in clear and cloudy conditions. Dilution effects will also vary with wind speed and direction. However, we assume that cloud coverage on any particular day does not, on average, correlate with cloud levels on the previous days. The oxidation of SO_2 to sulphate aerosol takes place over several days, so we assume that the aerosol retrievals presented here are representative of the average AOD for all synoptic conditions, i.e. that there is no systematic difference between aerosol burden in clear and cloudy conditions.

As aerosol and cloud properties are both dependent on the same meteorological processes, there is a potential for spurious correlation between AOD and cloud properties, unrelated to volcanic aerosol. For example, cyclones are associated with both increased cloud fraction (Field and Wood, 2007) and increased aerosol optical depth due to high relative humidity and wind speeds, resulting in elevated hygroscopic growth of aerosols (e.g. Seinfeld and Pandis, 1998) and, more importantly, increased sea spray emission (e.g., Grandey et al., 2011). As we use retrievals from the full range of atmospheric conditions such effects should have a significant impact on our results. False correlations between aerosol and cloud properties may also be introduced by analysis of satellite data over large regions containing significant variation in aerosol type, cloud regime and average synoptic conditions (Grandey and Stier, 2010). We limit the chance of our results being affected by spurious correlations due to spatial variations

ACPD
14, 2675–2716, 2014

in climate by limiting measurements to regions of up to only 4° across, the largest regional size recommended by Grandey and Stier (2010) for analysis of aerosol indirect effects. Only in data from the 800 km^2 (4°) surrounding Yasur do we observe a regional trend in aerosol properties that is systematic with wind direction.

4.3 Volcanic aerosol and cloud interaction

The impact of the additional CCN burden associated with volcanic emission depends strongly on synoptic conditions and the state of any pre-existing cloud (e.g. where level of supersaturation is low, volcanogenic aerosol will not have the capacity to act as CCN). We expect that cloud measurements over ocean will capture decks of marine stratocumulus, while those over land and in the islands' wakes may also include orographic clouds. As we select data just for lower tropospheric pressures our analysis does not account for the impact of volcanic gases and aerosols that escape the boundary layer. As these measurements are made from averaged retrievals, they contain contributions from days with a range of meteorological conditions. The mean values for cloud optical depth and droplet effective radius presented here therefore capture net conditions and may not bear a resemblance to the processes that took place on any particular day.

Ship track studies have identified marine cloud types and synoptic conditions most likely to support ship-track formation. Marine stratocumulus in particular have been observed to be susceptible to alteration by excess aerosol. Ship tracks are most commonly observed in low-level stratocumulus, where the aerosol plume is able to mix directly with an overlying cloud deck before major dispersal. Typical ship tracks form when the boundary layer is thin (< 800 m), wind speeds are moderate, relative humidity is high and the difference in temperature between air and sea is low (Durkee et al., 2000). The impact of additional CCN on orographic cloud has been less well studied, and conditions most likely to result in cloud brightening are unclear (Muhlbauer et al., 2010).

ACPD
14, 2675–2716, 2014

All of the islands investigated here are in regions where the free atmosphere is dominated by trade winds, except Tristan da Cunha, where westerlies dominate. The maximum impact of volcano on aerosol/clouds for our examples is immediately downwind of the edge of the island in each case and at pressure levels typical of boundary layer clouds. We consider the average conditions captured in Fig. 2c, g, k representative of an aerosol plume rising to meet an existing cloud deck at the boundary layer. Our measurements of time-averaged impact would be complemented by case-by-case analysis of volcanic ship tracks (e.g. Gassó, 2008) to improve our understanding of the influence of atmospheric conditions and emission characteristics on average cloud properties.

4.4 Extrapolating to the present and past global volcano indirect effect

Our approach builds on snapshot studies of cloud and aerosol interaction on particular days by providing an estimation of average volcanic impact over several years. This is a step towards the measurement of the long-term impact of persistent volcanic activity in the present day atmosphere. In the three test cases described here, we observe some general trends that could be extrapolated to other volcanoes. First, high average downwind AOD is linked with high background SO_2 flux. Although daily ground-based measurements of SO_2 do not correlate with daily satellite retrievals of AOD, average background SO_2 flux at the three volcanoes (Table 1) investigated here is proportional to time averaged upwind–downwind difference in AOD (Table 2, Fig. 2). Both the greatest upwind–downwind differences in AOD and CER and the greatest distance to minimum CER were found at Kīlauea, the volcano with the highest SO_2 flux.

Our observations at Kīlauea and Yasur alone capture the impact of about half of the SO_2 expected on average from isolated island volcanoes globally. Of the 49 continuously erupting volcanoes for which Andres and Kasgnoc (1998) present SO_2 fluxes, only 8 are islands further than ~ 50 km from the nearest land mass and together contribute ~ 14 % of the SO_2 flux in the compilation. The remaining SO_2 flux from continuously degassing volcanoes originates on the continents (24 volcanoes) or within ~ 50 km of the nearest large landmass (17 volcanoes). These “coastal” volcanoes, in-

ACPD
14, 2675–2716, 2014

cluding Etna, Bagana and Sakura-jima, emit almost ~ 50 % of global continuous emissions (Andres and Kasgnoc, 1998). Observations of a volcanic indirect effect in continental or coastal settings may be achievable using trajectory analysis of air parcels from the volcano to allow comparison of aerosol laden atmosphere to average background conditions. Our observations of a volcanic indirect effect at Piton de la Fournaise demonstrates that persistently active volcanoes without a constant SO_2 flux to the atmosphere also have an impact on local cloud properties. A complete inventory of tropospheric cloud alteration by volcanoes should therefore also include emission associated with minor explosions.

The volcanic indirect effect observed in this study is unlikely to be representative of the average present day impact of volcanoes worldwide. Importantly, the impact of additional aerosols on cloud microphysics is greater for pristine clouds than for polluted regions (e.g. Lohmann et al., 2005; Rosenfeld et al., 2008). The change in cloud droplet size downwind of Kīlauea, Yasur and Piton de la Fournaise is expected to be large relative to that for volcanoes that emit aerosol into heavily polluted cloud decks (e.g. Etna, Masaya). However, these observations of the most pristine parts of the Earth's present day atmosphere are likely to be the best observable analogue of pre-industrial aerosol effects.

5 Conclusions

A demonstrable volcanic indirect effect is observed at three persistently active volcanoes with different eruptive characteristics: Kīlauea (strong degassing), Yasur (Strombolian eruptions) and Piton de la Fournaise (minor explosions and lava flows). Within ~ 200 km distance of all volcanoes, we observed a time-averaged elevation in AOD (increase < 0.07) and lower CER (decrease < 8 µm) downwind of the volcano relative to upwind. The patterns in rotated cloud and aerosol data at three "control" islands showed no orographic effect of a magnitude sufficient to mask the changes in cloud properties observed at the degassing volcanoes.

ACPD
14, 2675–2716, 2014

Our approach of rotating MODIS and AATSR retrievals according to horizontal wind direction has allowed us to observe the net impact of volcanic activity over several years. It is appropriate for isolated volcanic islands, where both upwind and downwind retrievals are made over the ocean and other sources of aerosol, especially anthropogenic aerosol, are limited.

We estimate that our observations of the volcanic indirect effect originate from ∼ 7 % of the world's continuous volcanic SO_2 flux from Kīlauea and Yasur. We also demonstrate the impact of minor explosions on local cloud properties at Piton de la Fournaise. These examples provide some first steps towards automated global observation of the present day volcanic indirect effect. They also provide observations of aerosol indirect effect in the most pristine parts of the present day atmosphere.

Acknowledgements. We thank S. Gassó for useful discussions at the inception of this project and during manuscript preparation. S. K. Ebmeier is funded by the UK National Environmental Research Council through the COMET/NCEO and STREVA programmes. R. G. Grainger, T. A. Mather and E. Carboni are also supported by COMET/NCEO. GRAPE data are hosted by the BADC and MODIS data are hosted by NASA LAADS.

References

Ackerman, A. S., Toon, O. B., Taylor, J. P., Johnson, D. W., Hobbs, P. V., and Ferek, R. J.: Effects of aerosols on cloud albedo: evaluation of Twomey's parameterization of cloud susceptibility using measurements of ship tracks, J. Atmos. Sci., 57, 2684–2695, doi:10.1175/1520-0469(2000)057<2684:EOAOCA>2.0.CO;2, 2000. 2677

Ackerman, S., Holz, R., Frey, R., Eloranta, E., Maddux, B., and McGill, M.: Cloud detection with MODIS – Part 2: Validation, J. Atmos. Ocean. Tech., 25, 1073–1086, doi:10.1175/2007JTECHA1053.1, 2008. 2681

Albrecht, B.: Aerosols, cloud microphysics, and fractional cloudiness, Science, 245, 1227, doi:10.1126/science.245.4923.1227, 1989. 2677

Allen, A., Oppenheimer, C., Ferm, M., Baxter, P., Horrocks, L., Galle, B., McGonigle, A., and Duffell, H.: Primary sulfate aerosol and associated emissions from Masaya Volcano, Nicaragua, J. Geophys. Res., 107, 4682, doi:10.1029/2002JD002120, 2002. 2679

Andreae, M. O.: Aerosols before pollution, Science, 315, 50–51, doi:10.1126/science.1136529, 2007. 2677

Andres, R. and Kasgnoc, A.: A time-averaged inventory of subaerial volcanic sulfur emissions, J. Geophys. Res., 103, 25251–25261, doi:10.1029/98JD02091, 1998. 2678, 2680, 2687, 2688, 2689, 2696, 2697

Bani, P. and Lardy M.: Sulphur dioxide emission rates from Yasur volcano, Vanuatu archipelago, Geophys. Res. Lett., 34, L20309, doi:10.1029/2007GL030411, 2007. 2689

Bani, P., Oppenheimer, C., Allard, P., Shinohara, H., Tsanev, V., Carn, S., Lardy, M., and Garaebiti, E.: First estimate of volcanic SO_2 budget for Vanuatu island arc, J. Volcanol. Geoth. Res., 211, 36–46, doi:10.1016/j.jvolgeores.2011.10.005, 2012. 2689, 2690, 2706

Bhugwant, C., Siéja, B., Bessafi, M., Staudacher, T., and Ecormier, J.: Atmospheric sulfur dioxide measurements during the 2005 and 2007 eruptions of the Piton de La Fournaise volcano: implications for human health and environmental changes, J. Volcanol. Geoth. Res., 184, 208–224, doi:10.1016/j.jvolgeores.2009.04.012, 2009. 2690

Brenguier, J., Pawlowska, H., and Schüller, L.: Cloud microphysical and radiative properties for parameterization and satellite monitoring of the indirect effect of aerosol on climate, J. Geophys. Res., 108, 8632, doi:10.1029/2002JD002682, 2003. 2678

Campmany, E., Grainger, R. G., Dean, S. M., and Sayer, A. M.: Automatic detection of ship tracks in ATSR-2 satellite imagery, Atmos. Chem. Phys., 9, 1899–1905, doi:10.5194/acp-9-1899-2009, 2009. 2677, 2680

Carslaw, K. S., Lee, L. A., Reddington, C. L., Pringle, K. J., Rap, A., Forster, P. M., Mann, G. W., Spracklen, D. V., Woodhouse, M. T., Regayre, L., and Pierce, J. R.: Large contribution of natural aerosols to uncertainty in indirect forcing, Nature, 503, 67–71, 2013. 2677, 2679

Chen, Y.-C., Christensen, M. W., Xue, L., Sorooshian, A., Stephens, G. L., Rasmussen, R. M., and Seinfeld, J. H.: Occurrence of lower cloud albedo in ship tracks, Atmos. Chem. Phys., 12, 8223–8235, doi:10.5194/acp-12-8223-2012, 2012. 2678

Christensen, M. W. and Stephens, G. L.: Microphysical and macrophysical responses of marine stratocumulus polluted by underlying ships: evidence of cloud deepening, J. Geophys. Res.-Atmos., 116, D03201, doi:10.1029/2010JD014638, 2011. 2677

ACPD
14, 2675–2716, 2014

Coppola, D., Piscopo, D., Staudacher, T., and Cigolini, C.: Lava discharge rate and effusive pattern at Piton de la Fournaise from MODIS data, J. Volcanol. Geoth. Res., 184, 174–192, doi:10.1016/j.jvolgeores.2008.11.031, 2009. 2706

Dee, D. P., Uppala, S. M., Simmons, A. J., Berrisford, P., Poli, P., Kobayashi, S., Andrae, U., Balmaseda, M. A., Balsamo, G., Bauer, P., Bechtold, P., Beljaars, A. C. M., van de Berg, L., Bidlot, J., Bormann, N., Delsol, C., Dragani, R., Fuentes, M., Geer, A. J., Haimberger, L., Healy, S. B., Hersbach, H., Hólm, E. V., Isaksen, L., Kållberg, P., Köhler, M., Matricardi, M., McNally, A. P., Monge-Sanz, B. M., Morcrette, J.-J., Park, B.-K., Peubey, C., de Rosnay, P., Tavolato, C., Thépaut, J.-N., and Vitart, F.: The ERA-Interim reanalysis: configuration and performance of the data assimilation system, Q. J. Roy. Meteor. Soc., 137, 553–597, doi:10.1002/qj.828, 2011. 2682

Dentener, F., Kinne, S., Bond, T., Boucher, O., Cofala, J., Generoso, S., Ginoux, P., Gong, S., Hoelzemann, J. J., Ito, A., Marelli, L., Penner, J. E., Putaud, J.-P., Textor, C., Schulz, M., van der Werf, G. R., and Wilson, J.: Emissions of primary aerosol and precursor gases in the years 2000 and 1750 prescribed data-sets for AeroCom, Atmos. Chem. Phys., 6, 4321–4344, doi:10.5194/acp-6-4321-2006, 2006. 2680

Di Muro, A., Aiuppa, A., Burton, M., Metrich, N., Allard, P., Fougeroux, T., Giudice, G., and Guida, R.: Intra-eruptive gas emissions and shallow magma storage after the 2007 summit caldera collapse of Piton de la Fournaise, Reunion island, in: EGU General Assembly Conference Abstracts, EGU General Assembly Conference Abstracts, vol. 14, edited by: Abbasi, A. and Giesen, N., European Geophysical Union, Vienna, p. 2761, 2012. 2690, 2706

Durkee, P. A., Chartier, R. E., Brown, A., Trehubenko, E. J., Rogerson, S. D., Skupniewicz, C., Nielsen, K. E., Platnick, S., and King, M. D.: Composite ship track characteristics, J. Atmos. Sci., 57, 2542–2553, doi:10.1175/1520-0469(2000)057<2542:CSTC>2.0.CO;2, 2000. 2677, 2695

Eatough, D. J., Caka, F. M., and Farber, R. J.: The conversion of SO_2 to sulfate in the atmosphere, Israel Journal of Chemistry, 34, 301–314, 1995. 2678, 2694

Edmonds, M. and Gerlach, T.: The airborne lava–seawater interaction plume at Kīlauea Volcano, Hawaii, Earth Planet. Sc. Lett., 244, 83–96, doi:10.1016/j.epsl.2006.02.005, 2006. 2693

Elias, T. and Sutton, A. J.: Sulfur dioxide emission rates from Kilauea Volcano, Hawai'i, 2007–2010, US Geological Survey Open-File Report, 1107, 25 pp., 2012. 2687, 2688, 2706, 2714

ACPD
14, 2675–2716, 2014

Field, P. R., and Wood, R.: Precipitation and cloud structure in midlatitude cyclones, J. Climate, 20, 233–254, doi:10.1175/JCLI3998.1, 2007. 2694

Garofalo, K., Staudacher, T., Ferrazzini, V., Kowalski, P., Boissier, P., Dupont, A., Peltier, A., Villemant, B., and Boudon, G.: Eruptive SO_2-plume measurements at Piton de la Fournaise (Ile de la Réunion) by stationary NOVAC scanning MAX-DOAS instruments, in: EGU General Assembly Conference Abstracts, European Geophysical Union, Vienna, vol. 11, p. 12113, 2009. 2706

Gassó, S.: Satellite observations of the impact of weak volcanic activity on marine clouds, J. Geophys. Res.-Atmos., 113, D14S19, doi:10.1029/2007JD009106, 2008. 2679, 2680, 2682, 2696

Gouhier, M. and Coppola, D.: Satellite-based evidence for a large hydrothermal system at Piton de la Fournaise volcano (Reunion Island), Geophys. Res. Lett., 38, L02302, doi:10.1029/2010GL046183, 2011. 2690, 2693

Graf, H., Langmann, B., and Feichter, J.: The contribution of Earth degassing to the atmospheric sulfur budget, Chem. Geol., 147, 131–145, doi:10.1016/S0009-2541(97)00177-0, 1998. 2678

Grandey, B. S. and Stier, P.: A critical look at spatial scale choices in satellite-based aerosol indirect effect studies, Atmos. Chem. Phys., 10, 11459–11470, doi:10.5194/acp-10-11459-2010, 2010. 2694, 2695

Grandey, B. S., Stier, P., Wagner, T. M., Grainger, R. G., and Hodges, K. I.: The effect of extratropical cyclones on satellite-retrieved aerosol properties over ocean, Geophys. Res. Lett., 38, L13805, doi:10.1029/2011GL047703, 2011. 2694

Halmer, M., Schmincke, H., and Graf, H.: The annual volcanic gas input into the atmosphere, in particular into the stratosphere: a global data set for the past 100 years, J. Volcanol. Geoth. Res., 115, 511–528, doi:10.1016/S0377-0273(01)00318-3, 2002. 2678

Hansen, J., Sato, M., and Ruedy, R.: Radiative forcing and climate response, J. Geophys. Res., 102, 6831–6864, doi:doi:10.1029/96JD03436, 1997. 2677

Houze, R. A. J.: Cloud dynamics, vol. 53, Access Online via Elsevier, Academic Press, Inc., San Diego, California, 1994. 2686

Huang, H., Thomas, G. E., and Grainger, R. G.: Relationship between wind speed and aerosol optical depth over remote ocean, Atmos. Chem. Phys., 10, 5943–5950, doi:10.5194/acp-10-5943-2010, 2010. 2691

ACPD
14, 2675–2716, 2014

Jiusto, J.: Aerosol and cloud microphysics measurements in Hawai'i, Tellus, 19, 359–368, 1967. 2683, 2687

Khokhar, M., Frankenberg, C., van Roozendael, M., Beirle, S., Kühl, S., Richter, A., Platt, U., and Wagner, T.: Satellite observations of atmospheric SO_2 from volcanic eruptions during the time-period of 1996–2002, Adv. Space Res., 36, 879–887, doi:10.1016/j.asr.2005.04.114, 2005. 2690

Lee, L. A., Pringle, K. J., Reddington, C. L., Mann, G. W., Stier, P., Spracklen, D. V., Pierce, J. R., and Carslaw, K. S.: The magnitude and causes of uncertainty in global model simulations of cloud condensation nuclei, Atmos. Chem. Phys., 13, 8879–8914, doi:10.5194/acp-13-8879-2013, 2013. 2679

Lohmann, U. and Feichter, J.: Global indirect aerosol effects: a review, Atmos. Chem. Phys., 5, 715–737, doi:10.5194/acp-5-715-2005, 2005. 2677, 2693, 2697

Martin, G., Ringer, M., Pope, V., Jones, A., Dearden, C., and Hinton, T.: The physical properties of the atmosphere in the new hadley centre global environmental model (HADGEM1) – Part 1: Model description and global climatology, J. Climate, 19, 1274–1301, doi:10.1175/JCLI3636.1, 2006. 2680

Martin, R., Mather, T., Pyle, D., Power, M., Allen, A., Aiuppa, A., Horwell, C., and Ward, E.: Composition-resolved size distributions of volcanic aerosols in the Mt. Etna plumes, J. Geophys. Res., 113, D17211, doi:10.1029/2007JD009648, 2008. 2679

Mather, T., McCabe, J., Rai, V., Thiemens, M., Pyle, D., Heaton, T. H. E., Sloane, H. J., and Fern, G. R.: Oxygen and sulfur isotopic composition of volcanic sulfate aerosol at the point of emission, J. Geophys. Res., 111, D18205, doi:10.1029/2005JD006584, 2006. 2678

Mather, T., Witt, M., Pyle, D., Quayle, B., Aiuppa, A., Bagnato, E., Martin, R., Sims, K., Edmonds, M., Sutton, A., and Ilyinskaya, E.: Halogens and trace metal emissions from the ongoing 2008 summit eruption of Kīlauea volcano, Hawai'i, Geochim. Cosmochim. Ac., 83, 292–323, doi:10.1016/j.gca.2011.11.029, 2012. 2679, 2688

Mather, T. A., Pyle, D. M., and Oppenheimer, C.: Tropospheric volcanic aerosol, Geoph. Monog. Series, 139, 189–212, 2003. 2678

Mather, T. A., Tsanev, V. I., Pyle, D. M., McGonigle, A. J. S., Oppenheimer, C., and Allen, A. G.: Characterization and evolution of tropospheric plumes from Lascar and Villarrica volcanoes, Chile, J. Geophys. Res.-Atmos., 109, D21303, doi:10.1029/2004JD004934, 2004. 2679, 2680

ACPD
14, 2675–2716, 2014

Métrich, N., Allard, P., Aiuppa, A., Bani, P., Bertagnini, A., Shinohara, H., Parello, F., Di Muro, A., Garaebiti, E., Belhadj, O., and Massare, D.: Magma and volatile supply to post-collapse volcanism and block resurgence in Siwi Caldera (Tanna Island, Vanuatu Arc), J. Petrol., 52, 1077–1105, doi:10.1093/petrology/egr019, 2011. 2693

Muhlbauer, A., Hashino, T., Xue, L., Teller, A., Lohmann, U., Rasmussen, R. M., Geresdi, I., and Pan, Z.: Intercomparison of aerosol-cloud-precipitation interactions in stratiform orographic mixed-phase clouds, Atmos. Chem. Phys., 10, 8173–8196, doi:10.5194/acp-10-8173-2010, 2010. 2695

Oppenheimer, C., Scaillet, B., and Martin, R. S.: Sulfur degassing from volcanoes: source conditions, surveillance, plume chemistry and earth system impacts, Rev. Mineral. Geochem., 73, 363–421, doi:10.2138/rmg.2011.73.13, 2011. 2678

Peltier, A., Bachèlery, P., and Staudacher, T.: Magma transport and storage at Piton de La Fournaise (La Réunion) between 1972 and 2007: a review of geophysical and geochemical data, J. Volcanol. Geoth. Res., 184, 93–108, doi:10.1016/j.jvolgeores.2008.12.008, 2009. 2690

Peters, K., Quaas, J., and Graßl, H.: A search for large-scale effects of ship emissions on clouds and radiation in satellite data, J. Geophys. Res.-Atmos., 116, D24205, doi:10.1029/2011JD016531, 2011. 2677

Platnick, S.: Vertical photon transport in cloud remote sensing problems, J. Geophys. Res.-Atmos., 105, 22919–22935, doi:10.1029/2000JD900333, 2000. 2685

Platnick, S., King, M. D., Ackerman, S. A., Menzel, W. P., Baum, B. A., Riédi, J. C., and Frey, R. A.: The MODIS cloud products: algorithms and examples from Terra, IEEE T. Geosci. Remote, 41, 459–473, doi:10.1109/TGRS.2002.808301, 2003. 2681, 2693

Porter, J. N., Horton, K. A., Mouginis-Mark, P. J., Lienert, B., Sharma, S. K., Lau, E., Sutton, A. J., Elias, T., and Oppenheimer, C.: Sun photometer and lidar measurements of the plume from the Hawaii Kilauea Volcano Pu'u O'o vent: aerosol flux and SO_2 lifetime, Geophys. Res. Lett., 29, 1783, doi:10.1029/2002GL014744, 2002. 2688

Poulsen, C. A., Siddans, R., Thomas, G. E., Sayer, A. M., Grainger, R. G., Campmany, E., Dean, S. M., Arnold, C., and Watts, P. D.: Cloud retrievals from satellite data using optimal estimation: evaluation and application to ATSR, Atmos. Meas. Tech., 5, 1889–1910, doi:10.5194/amt-5-1889-2012, 2012. 2681

Remer, L. A., Kaufman, Y., Tanré, D., Mattoo, S., Chu, D., Martins, J., Li, R.-R., Ichoku, C., Levy, R., Kleidman, R., Eck, T. F., Vermote, E. and Holben, B. N.: The MODIS aerosol algo-

ACPD
14, 2675–2716, 2014

rithm, products, and validation, J. Atmos. Sci., 62, 947–973, doi:10.1175/JAS3385.1, 2005. 2681, 2683

Robock, A.: Pinatubo eruption: The climatic aftermath, Science, 295, 1242–1244, doi:10.1126/science.1069903, 2002. 2678

Rosenfeld, D., Lohmann, U., Raga, G., O'Dowd, C., Kulmala, M., Fuzzi, S., Reissell, A., and Andreae, M.: Flood or drought: how do aerosols affect precipitation?, Science, 321, 1309–1313, doi:10.1126/science.1160606, 2008. 2697

Sassen, K.: Evidence for liquid-phase cirrus cloud formation from volcanic aerosols: climatic implications, Science, 257, 516–519, doi:10.1126/science.257.5069.516, 1992. 2678

Sayer, A. M., Thomas, G. E., and Grainger, R. G.: A sea surface reflectance model for (A)ATSR, and application to aerosol retrievals, Atmos. Meas. Tech., 3, 813–838, doi:10.5194/amt-3-813-2010, 2010. 2681, 2692

Sayer, A. M., Poulsen, C. A., Arnold, C., Campmany, E., Dean, S., Ewen, G. B. L., Grainger, R. G., Lawrence, B. N., Siddans, R., Thomas, G. E., and Watts, P. D.: Global retrieval of ATSR cloud parameters and evaluation (GRAPE): dataset assessment, Atmos. Chem. Phys., 11, 3913–3936, doi:10.5194/acp-11-3913-2011, 2011. 2685

Sayer, A., Smirnov, A., Hsu, N., and Holben, B.: A pure marine aerosol model, for use in remote sensing applications, J. Geophys. Res.-Atmos., 117, D05213, doi:10.1029/2011JD016689, 2012. 2691

Schmidt, A., Carslaw, K. S., Mann, G. W., Wilson, M., Breider, T. J., Pickering, S. J., and Thordarson, T.: The impact of the 1783–1784 AD Laki eruption on global aerosol formation processes and cloud condensation nuclei, Atmos. Chem. Phys., 10, 6025–6041, doi:10.5194/acp-10-6025-2010, 2010. 2678

Schmidt, A., Carslaw, K. S., Mann, G. W., Rap, A., Pringle, K. J., Spracklen, D. V., Wilson, M., and Forster, P. M.: Importance of tropospheric volcanic aerosol for indirect radiative forcing of climate, Atmos. Chem. Phys., 12, 7321–7339, doi:10.5194/acp-12-7321-2012, 2012. 2679, 2680

Seinfeld, J. H. and Pandis, S. N.: Atmospheric Chemistry and Physics, John Wiley, Hoboken, NJ, 1326 pp., 1998. 2694

Shi, Y., Zhang, J., Reid, J. S., Holben, B., Hyer, E. J., and Curtis, C.: An analysis of the collection 5 MODIS over-ocean aerosol optical depth product for its implication in aerosol assimilation, Atmos. Chem. Phys., 11, 557–565, doi:10.5194/acp-11-557-2011, 2011. 2692

ACPD
14, 2675–2716, 2014

Siebert, L. and Simkin, T.: Volcanoes of the World: an Illustrated Catalog of Holocene Volcanoes and their Eruptions, Smithsonian Institution, Global Volcanism Program Digital Information Series, GVP-3, Smithsonian Institution, Washington D.C., available at: http://www.volcano.si.edu/world/ (last access: 20 November 2013), 2002. 2682, 2691

Siebert, L., Simkin, T., and Kimberly, P.: Volcanoes of the World, 3rd edn., Univeristy of California Press, Berkley, 2010. 2691, 2706

Smirnov, A., Sayer, A. M., Holben, B. N., Hsu, N. C., Sakerin, S. M., Macke, A., Nelson, N. B., Courcoux, Y., Smyth, T. J., Croot, P., Quinn, P. K., Sciare, J., Gulev, S. K., Piketh, S., Losno, R., Kinne, S., and Radionov, V. F.: Effect of wind speed on aerosol optical depth over remote oceans, based on data from the Maritime Aerosol Network, Atmos. Meas. Tech., 5, 377–388, doi:10.5194/amt-5-377-2012, 2012. 2691, 2692

Thomas, G. E., Poulsen, C. A., Sayer, A. M., Marsh, S. H., Dean, S. M., Carboni, E., Siddans, R., Grainger, R. G., and Lawrence, B. N.: The GRAPE aerosol retrieval algorithm, Atmos. Meas. Tech., 2, 679–701, doi:10.5194/amt-2-679-2009, 2009. 2681

Tulet, P. and Villeneuve, N.: Large scale modeling of the transport, chemical transformation and mass budget of the sulfur emitted during the April 2007 eruption of Piton de la Fournaise, Atmos. Chem. Phys., 11, 4533–4546, doi:10.5194/acp-11-4533-2011, 2011. 2690, 2691

Twomey, S.: The influence of pollution on the shortwave albedo of clouds, J. Atmos. Sci., 34, 1149–1152, 1977. 2677

Yuan, T., Remer, L. A., and Yu, H.: Microphysical, macrophysical and radiative signatures of volcanic aerosols in trade wind cumulus observed by the A-Train, Atmos. Chem. Phys., 11, 7119–7132, doi:10.5194/acp-11-7119-2011, 2011. 2679, 2680, 2682, 2683, 2688

ACPD
14, 2675–2716, 2014

Table 1. Location, physical properties, degassing flux and eruptive character for volcanoes and "control" islands discussed in this study.

Volcano/Island	Latitude (°)	Longitude (°)	Maximum diameter of island (km)	Summit height (m)	"Background" SO_2 flux ($Mg\,day^{-1}$)	Activity 2002–2008
Volcanoes						
Kīlauea	19.42	−155.29	130	1222	1800 (2002–2007)[a]	Effusive lava flows, lava lake
Yasur	−19.53	169.44	40	361	633 (2004–2008)[b]	Strombolian
Piton de la Fournaise	−21.23	55.71	70	2632	Inter-eruptive flux is very low[c]	Minor explosions and basaltic flows[d]
"Control Islands"						
Fiji	−17.63	178.02	140	1324	–	–
Ofu-olosega	−14.18	169.62	9	639	–	–
Tristan da Cuhna	−37.09	−12.28	12	2060	–	–

"SO_2 flux" refers to time-averaged values of emission not associated with explosions as found from measurements presented by:
[a] Elias and Sutton (2012), [b] Bani et al. (2012) and [c] Coppola et al. (2009); Garofalo et al. (2009); Di Muro et al. (2012). [d] Eruptions at Piton de la Fournaise occurred during: October 2010–December 2010, November 2009–January 2010, September 2008–February 2009, July 2006–May 2007, February 2005, May 2004–October 2004, May 2003–January 2004 and November 2002–December 2002, Siebert et al. (2010).

ACPD
14, 2675–2716, 2014

Table 2. Average difference in upwind and downwind cloud and aerosol properties for MODIS-Aqua, Terra and AATSR retrievals for volcanoes discussed in this study.

Volcano		AOD upwind[b]	peak AOD downwind	COD upwind[a]	COD downwind[c]	CER (µm) upwind[a]	min. CER (µm) downwind	peak distance[d] (km)
Kīlauea	Aqua	0.11	0.18	9	10	22	14	~ 100
	Terra	0.11	0.17	8	10	22	15	~ 100
	AATSR	0.10	0.17	10	11	19	14	~ 80
Yasur	Aqua	0.09	0.13	13	14	21	19	~ 40
	Terra	0.09	0.12	13	13	22	18	~ 40
	AATSR	0.08	0.15	14	14	20	19	~ 50
Piton de la Fournaise	Aqua	0.11	0.12	10	12	21	17	~ 50
	Terra	0.11	0.12	10	11	22	18	~ 40
	AATSR	0.10	0.16	13	13	19	17	~ 50

[a] Peak AOD and minimum CER refer to the highest and lowest values found downwind of the volcano respectively. Cloud top pressures are between 860 and 440 mb. [b] Average value upwind of the volcano (−400 to 0 km), [c] Average value downwind of the volcano (0 to 400 km), [d] "peak distance" refers to the approximate distance of peak AOD and lowest CER downwind from the volcanic vent.

ACPD
14, 2675–2716, 2014

Table 3. Regression parameters for wind speed and AOD at 550 nm from mean daily values within 50 km of the island edge with one sigma error.

Volcano	Instrument	gradient (km^{-1})	intercept
Kīlauea	Aqua	0.005 ± 0.003	0.08 ± 0.03
Yasur	Aqua	0.004 ± 0.003	0.08 ± 0.02
Piton de la Fournaise	Aqua	0.003 ± 0.003	0.09 ± 0.02

ACPD
14, 2675–2716, 2014

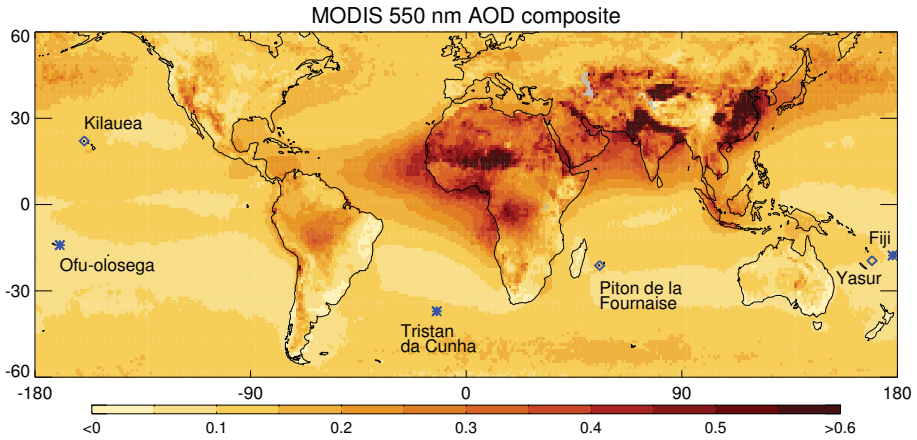

Fig. 1. The multiannual mean (2002–2008) of MODIS Aqua AOD at 550 nm, using Dark Target and ocean datasets, with Deep Blue to fill in gaps over land. Grey indicates that there is no data. Volcano locations are indicated by blue diamonds, "control" islands by blue crosses.

ACPD
14, 2675–2716, 2014

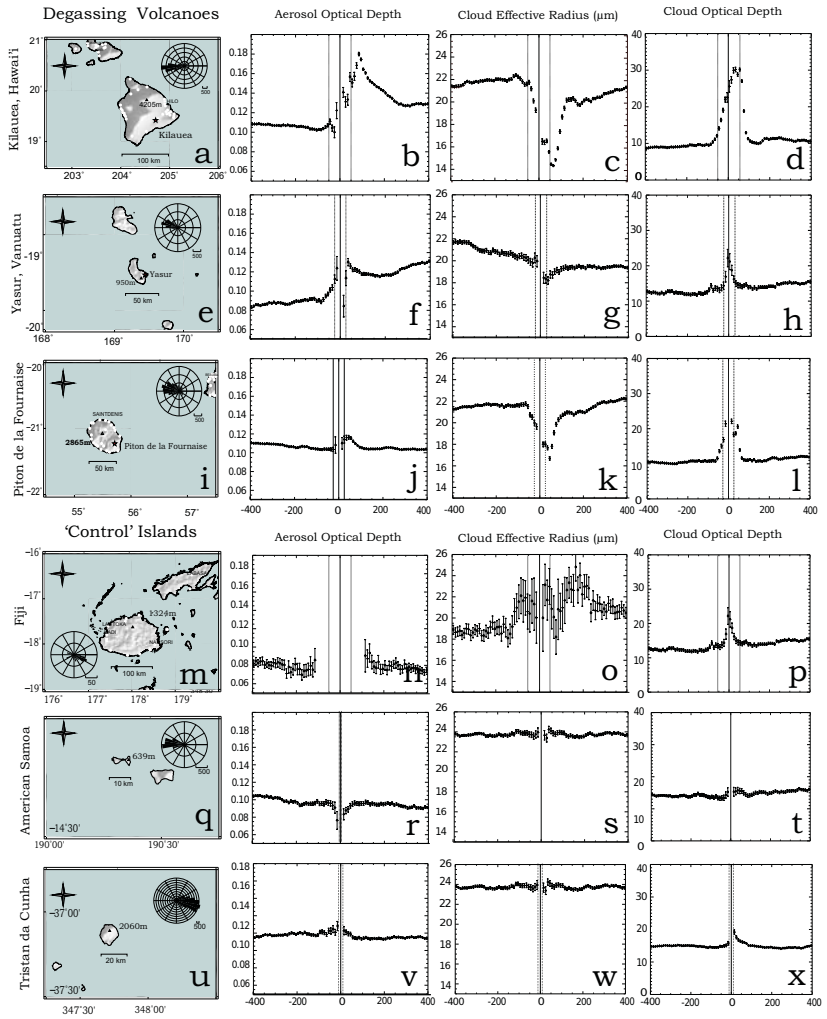

ACPD
14, 2675–2716, 2014

Passive volcanic degassing and cloud properties

S. K. Ebmeier et al.

Fig. 2. Profiles of average aerosol and cloud properties upwind and downwind of the degassing volcano: Kīlauea, Hawai'i **(a–d)**; Yasur, Vanuatu **(e–h)** and Piton de la Fournaise, Réunion **(i–l)** and at "control" islands: Fiji, West Pacific **(m–p)**; American Samoa, West Pacific **(q–t)** and Tristan da Cunha, South Atlantic **(u–x)**. Profile values are the average of arcs of $\frac{\pi}{2}$ at equal distance upwind and downwind from the volcano vent for MODIS Aqua data from between 2002 and 2008. Error bars show one standard error for this average and are generally larger for low sample sizes. Positive values on the x axis are downwind, negative upwind. Wind roses **(a, e, i, m, q, u)** show daily ECMWF wind directions, with black bars showing the directions towards which the wind was blowing. Topography is from NASA's Shuttle Radar Topography Mission (SRTM). The maximum diameter of the islands are indicated on the parameter plots as black dashed lines.

ACPD
14, 2675–2716, 2014

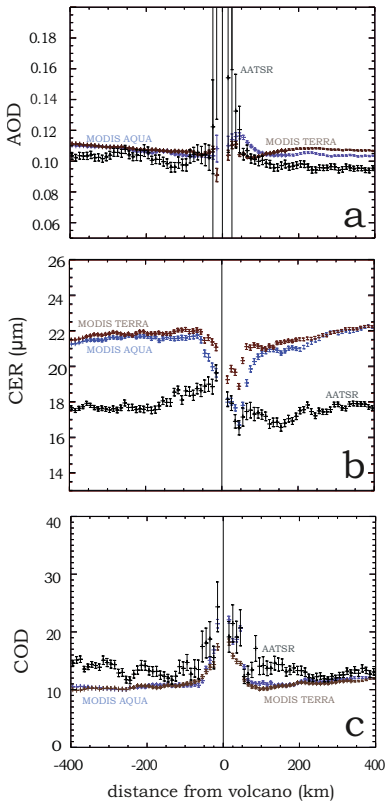

Fig. 3. Comparison of AOD, CER and COD values found from MODIS instruments and AATSR for data between 2002 and 2008 at Piton de la Fournaise, Réunion. MODIS Aqua data are plotted in blue, Terra in brown and AATSR in black. Profile values are the average of arcs of $\frac{\pi}{2}$ at equal distance upwind and downwind from the volcano vent. Error bars show one standard error in this average. Positive values on the *x* axis are downwind, negative upwind.

ACPD
14, 2675–2716, 2014

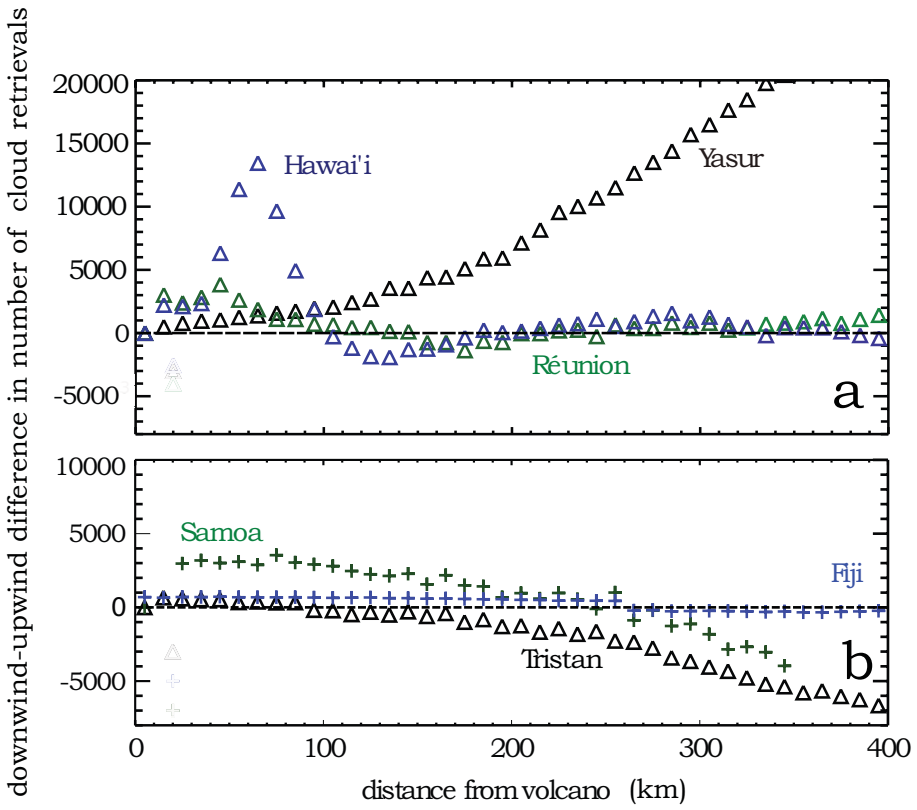

Fig. 4. Plots of the difference between numbers of cloud retrievals (cloud fraction > 0.2) downwind and upwind of volcanic vents **(a)** and island summits **(b)**. At Hawai'i, and to some extent Réunion, there is a notable increase in the number of cloud retrievals made downwind relative to upwind within 100 km of the island.

ACPD
14, 2675–2716, 2014

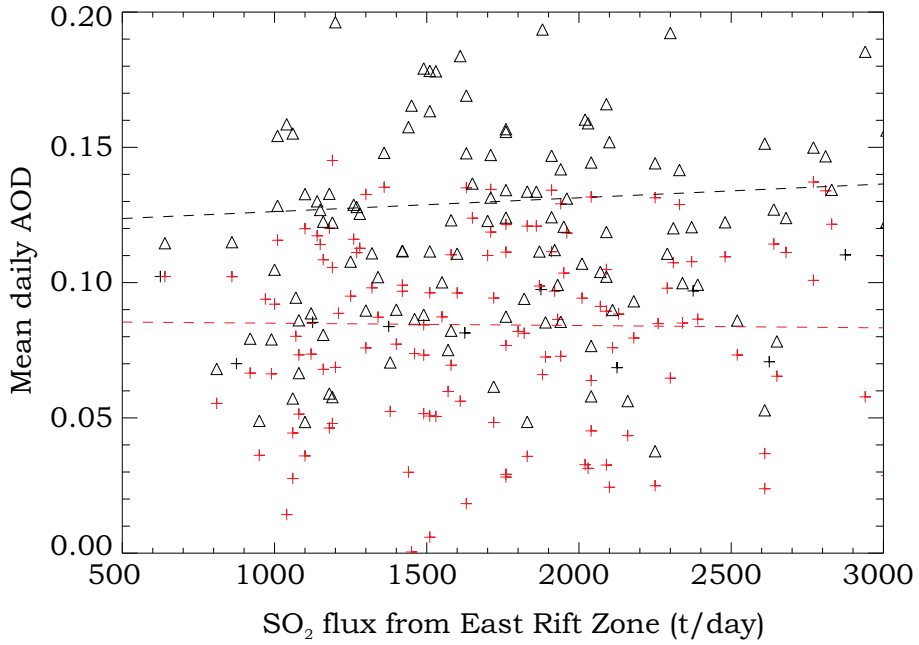

Fig. 5. Comparison of SO_2 flux from the East Rift as reported by (Elias and Sutton, 2012), with AOD (550 nm) measurements from MODIS Aqua on the same day. The lack of relationship between ground and satellite-based measurements may be due to several factors including dilution effects and differences in measurement times. Black triangles show MODIS AOD retrievals and the black dashed line indicates linear regression line. The red crosses show AOD values after de-trending for a linear relationship with windspeed, as demonstrated in Fig. 6. The red dashed line shows corrected linear regression.

ACPD
14, 2675–2716, 2014

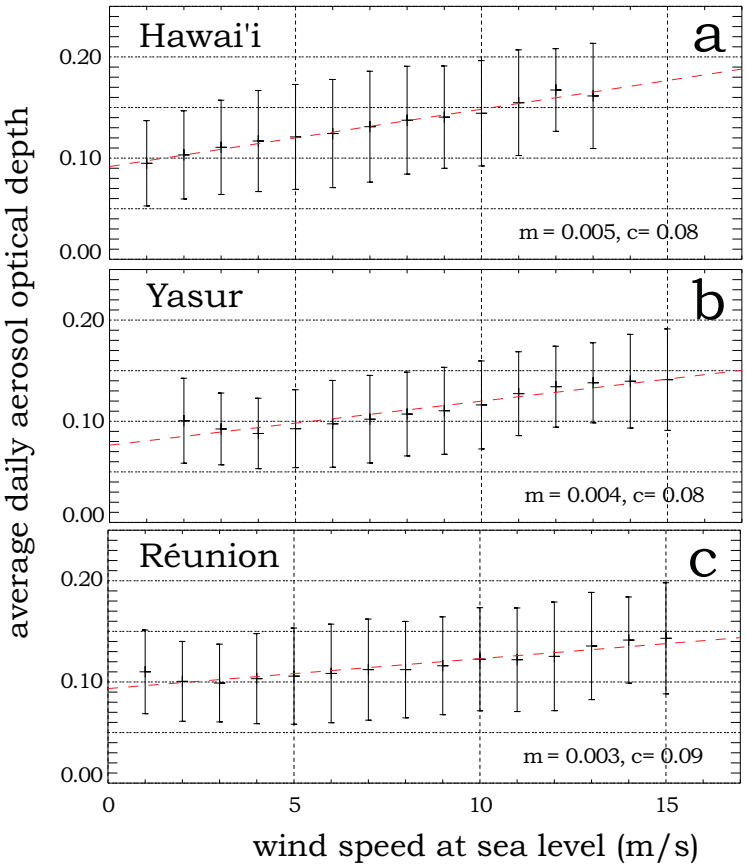

Fig. 6. Daily average AOD at 550 nm measured from MODIS, Aqua between 2002 and 2008 within 50 km of the coasts of **(a)** Hawai'i, **(b)** Yasur and **(c)** Réunion plotted as a function of horizontal wind speed at sea level from ECMWF. Error bars show the standard deviation in AODs for bin intervals of 1 m s^{-1}.

ACPD
14, 2675–2716, 2014

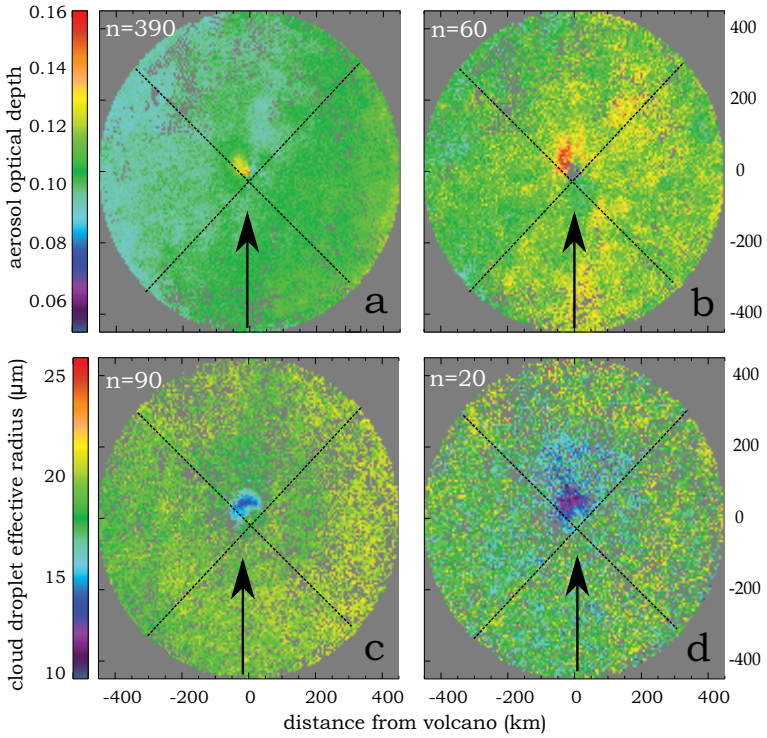

Fig. 7. Scatterplots show the average of rotated MODIS Aqua AOD (**a** and **b**) and CER (**c** and **d**) at Piton de la Fournaise during inter-eruptive (**a** and **c**) and eruptive (**b** and **d**) periods, 2002–2008. Cloud top pressures are 860–440 mb. The volcano summit is at (0,0) and arrows indicate wind direction. Downwind is the upper quadrant in each case. "*n*" values refer to the sample size in each image. Only data where sample sizes exceed 15 and relative standard deviations are less than 10 % are shown.

ACPD
14, 2675–2716, 2014